IAHR AIRH
Taylor & Francis
Taylor & Francis Group

Journal of Hydraulic Research Vol. 48, No. 4 (2010), pp. 476–482
doi:10.1080/00221686.2010.507001

Research paper

Flow characteristics of bottom outlets with moving gates

BIJAN DARGAHI (IAHR Member), Associate Professor, *Division of Hydraulic Engineering, the Royal Institute of Technology (KTH-LWR), Stockholm, Sweden*.
Email: bijan@kth.se

ABSTRACT
This study investigates the discharge characteristics of a bottom outlet with a moving gate by *Flow*3D. Experimental results for a scale model outlet of the Aswan Dam, Egypt, were used. Two different flow features were found. Pressurized flow established if the flume was filled and then the gate was slowly opened. However, a free surface flow occurred if the gate was fully opened and the entire flume was slowly flooded with water. The numerical simulations successfully captured the two flow patterns as well as the discharges and water surface profiles. The discharges were predicted with sufficient accuracy using the first-order momentum advection scheme. In comparison with the k-ε turbulence model, the Re-Normalization Group model yields the best agreement with the experiments. The model performed with similar accuracy for both model and prototype cases.

Keywords: Bottom outlet, CFD simulation, moving gate, three-dimensional model, VOF model

1 Introduction

Successful design and operation of hydraulic structures require effective and reliable tools to be applied to a variety of problems, including spillways, intakes, or bottom outlets. These flows share a complex character due to three-dimensional (3D) effects, surface waves, and air entrainment. The main concerns are related to accurate estimates of discharge coefficients, frictional losses, details of local flow patterns, position of the free surface, and air entrainment. Until recently, hydraulic scale model tests have served as principal approach. The latest improvements in Computational Fluid Dynamics (CFD) promote their use in place of scale models. For CFD to become reliable and acceptable as a design tool, the results must be carefully validated using experimental data. Recent CFD works concerning spillways are due to Olsen and Kjellesvig (1998), Unami *et al.* (1999), Ho *et al.* (2001, 2006), Savage and Johnson (2001a, 2001b), Bhajantri *et al.* (2007), Griffith *et al.* (2007), and Mehmet *et al.* (2009). Unami *et al.* (1999) developed a two-dimensional (2D) numerical model for spillway flows. They found a reasonable agreement with experimental data. Savage and Johnson (2001a, 2001b) presented a 2D simulation of flow over an ogee spillway using a commercial CFD code (Flow3D 2006). They found good agreement with experiments for both pressure and discharge. Ho *et al.* (2001) used Flow3D to model eight scaled physical models of spillway upgrade projects in Australia, successfully validating Flow3D against physical models. Griffith *et al.* (2007) extended the application of Flow3D to the stability analysis of Wanapum Spillway, located on Columbia River in Washington State. Having estimated pressures for the Probable Maximum Flood (PMF) condition, they concluded that the conventional stability analysis approach underestimated the sliding safety factor by 40–50%. All these studies confirm successful modelling of spillway flows by CFD.

A new CFD application to a bottom outlet structure with a moving gate is presented herein. Its objective was to investigate the flow features of the bottom outlet with a moving gate. In scale model tests, two different flow features were observed. Pressurized flow resulted if the flume was filled and then the gate was slowly opened, whereas a free surface flow appeared if the gate was fully opened and the entire flume was slowly flooded with water. The numerical simulations successfully captured these two flow features as well as the discharges and water surface profiles.

2 Experiments

The experiments dealt with the hydraulic model studies for determining the discharge capacity of one of the bottom outlets of Aswan Dam, Egypt, involving a movable gate (Cederwall and Bergh 1982). Two different flow features were found (Fig. 1):

Revision received 7 May 2010/Open for discussion until 28 February 2011.

ISSN 0022-1686 print/ISSN 1814-2079 online
http://www.informaworld.com

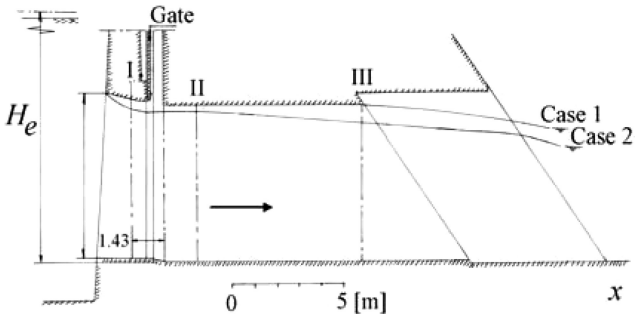

Figure 1 Cross-section of lower part of bottom outlet showing water surface profiles: Case 1 and Case 2, units in [m] at prototype scale

(1) pressurized flow was found if the flume was filled and then the gate was slowly opened (Case 1), and (2) free surface flow if the gate was fully opened and the entire flume was slowly flooded with water (Case 2).

Note that H_e is the upstream flow depth and a the bottom outlet opening. The main model was partly made in plywood of smooth, painted walls, and partly in transparent plastic using a geometrical scale of 1:22. Its surface roughness was retained with a Manning coefficient $n = 0.013\ \mathrm{m}^{-1/3}$ s corresponding to an equivalent roughness height of 0.72 mm, as computed from the Strickler formula (Townson 1991). The scale model was placed in a glass walled, recirculating hydraulic flume that is 0.6 m wide, 1.2 m deep, and 40 m long. The discharge was measured with a calibrated rectangular, sharp-crested weir to $\pm 5\%$. The downstream flow was always supercritical. The Froude law-based scales for velocity, discharge, and pressure were $1{:}22^{1/2}$, $1{:}22^{5/2}$, and 1:22, respectively. Figure 1 shows the cross-section of the lower intake portion. The upstream water levels were measured at $x = -0.3$ m, where x is the streamwise distance, using a pressure tap and two manometers of $\pm$(0.1 to 0.2) mm accuracy. The water surface profiles were measured from outside along the glass wall using a ruler from $x = 0.18$ to $x = 1.5$ m. These records were less reliable and had an estimated accuracy of ± 3 mm. The velocity distributions and pressures were also measured at section I (Fig. 1). All measurements were taken along the centre line of symmetry, i.e. at $y = 0.159$ m, where y denotes spanwise distance. For velocity measurements, a miniature velocity meter of 8 mm diameter and $\pm 5\ \mathrm{cm\ s}^{-1}$ accuracy was used. A Prandtl tube with an external diameter of 5 mm was used for static pressure measurements, involving a total error between 3% and 7%. The experiments were conducted for both fully opened and partially opened gates.

3 Numerical model

Flow3D, which is a general purpose CFD program for modelling multi-physics flow problems, heat transfer, and solidification, was used herein, based on the Finite-Volume Method to solve the full 3D Reynolds Averaged Navier–Stokes equations of fluid motion in Cartesian coordinates (Flow3D 2006). Flow3D was previously validated for different types of spillway flows (Ho *et al.* 2001, 2006, Savage and Johnson 2001a, 2001b, Griffith *et al.* 2007). The free surface is modelled using the Volume Of Fluid (VOF) method. The strength of Flow3D lies with its full implementation of the VOF model as opposed to Partial Volume Of Fluid. In Flow3D, to capture the model geometry and the obstacle in a rectangular domain, the Fraction Area/Volume Obstacle Representation (FAVOR) method was used in analogy to the VOF model (Hirt and Nichols 1981, Hirt and Sicilian 1985, Hirt 1992). The Re-Normalization Group (RNG) turbulence and the air-entrainment models were used; further, the k-ε turbulence model was also investigated.

3.1 *Model geometry and computational grid*

The scale model geometry was reproduced using AUTOCAD. The number of grids in (x,y,z) was varied in three different ranges, i.e. 175 × 10 × 75, 280 × 16 × 120, and 210 × 16 × 120, corresponding to a uniform mesh size in the range of 0.01–0.016 m in the (x,y) directions. In vertical direction, two different mesh resolutions were used. Non-uniform grid spacing from 0.3 to 0.9 mm was used adjacent to the bottom wall of the outlet corresponding to a non-dimensional wall distance between 30 and 100. Above the boundary layer, the mesh size ranged from 0.01 to 0.016 m. A resolution of 0.016 m corresponds to 175 × 10 × 75 (Fig. 2). It was impossible to obtain similar boundary layer grid resolutions for the prototype due to excessive grid points. The smallest possible grid size was 4 mm. To test grid dependency, the simulations were started with coarser grid sizes in the range 0.05–0.02 m. The flow symmetry along the centre plane was used to model half of the structure.

3.2 *Boundary conditions*

The upstream boundary was defined as hydrostatic pressure with various prototype energy heads from $H_e = 105$–113 m (Table 1). In Case 1, hydrostatic pressure was defined by setting H_e. In Case 2, a transient value of H_e was used. An

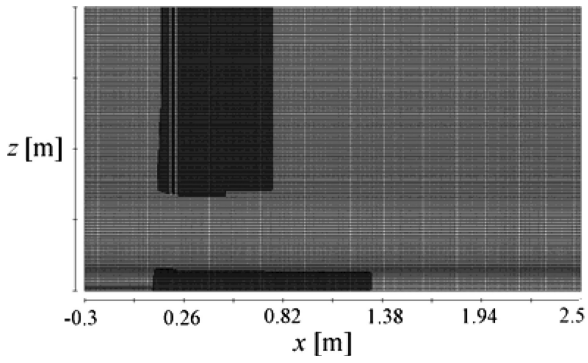

Figure 2 Cartesian grid in (x,z) plane in model scale 1:22

Table 1 Experimental results prototype and model scales

H_e, reservoir level (m)		Q, discharge Case 1 ($m^3\ s^{-1}$)		Q, discharge Case 2 ($m^3\ s^{-1}$)	
Prototype	Model	Prototype	Model	Prototype	Model
113	1.045	233	0.103	214	0.094
110	0.909	207	0.091	192	0.085
107	0.773	178	0.078	165	0.073
105	0.682	155	0.068	142	0.063

outflow boundary was set at the outlet where the flow was supercritical. The inlet turbulence properties were defined in terms of turbulent kinetic energy and dissipation rate (Dargahi 2004). The turbulent length scale was taken as $L = 0.07L$ (Casey and Wintergerste 2000), where L = relevant flow length, taken as the mean flow depth or the hydraulic radius at section I. The acceleration of gravity was applied in the negative z-direction. The wall roughness was set using the roughness height computed from the Strickler formula.

3.3 *Initial conditions*

The initial conditions were defined differently for two cases. In Case 1, a fluid region was defined upstream of the closed gate that filled the entire upstream portion of the model, equal to H_e (Table 1). The implementation of a static boundary condition maintained a constant fluid height (energy head). Gradually opening the gate, the fluid discharged into the model under the force of gravity. In Case 2, the initial fluid region covered the entire model to a depth of 2 cm. The void initial pressure was set to the atmospheric pressure in both cases.

3.4 *Modelling moving gate*

The gate movement was modelled using the General Moving Object (GMO) model that required the motion specification. A linear translation in the negative z-direction was used herein. To model moving objects, the GMO model also uses the FAVOR method.

3.5 *Numerical solver*

The simulations were run using the implicit solver Generalized Minimum Residual method (Flow3D 2006), which is highly accurate and efficient for a wide range of problems. The selected discretization method was the first-order momentum advection formulation. However, for Case 1 ($H_e = 0.682$ m), simulations were done using both first- and second-order discretizations for both the scaled model and the prototype. The initial time step was set to 0.003 s.

The transient flow simulations were done in both the model and prototype scales for Cases 1 and 2, using $H_e = 105$, 107, 110, and 113 m (prototype scale). In Case 1, the gate was raised gradually from its closed position at the same speed as in the experiments, i.e. 0.67 m s^{-1}. The water then started to flood the model, and the gate was completely opened within 60 s. To reach a steady-state solution, the simulations were continued for 320 s. For prototype simulations, the speed was scaled up with time scale factor, i.e. 1:4.69. In Case 2, the height of the initial fluid region was increased linearly at 2 s intervals until it reached the required height after 60 s. The simulations were continued for 320 s. The discharge characteristics were also studied for partial closure of the gate. These simulations were done for $H_e = 113$ m at 10 different gate openings that were increased at a rate of 10% in height (Fig. 1). The effects of the following variables on the solution were studied:

(1) equivalent roughness height varied between 0.3 and 0.72 mm (model scale), where the lower range corresponds to a hydraulically smooth, and the upper to a rough surface
(2) turbulent length scale varied between 0.073 and 0.338 m (model scale)
(3) choice of advection method (first and second orders)
(4) influence of turbulence model (k-ε and RNG)
(5) influence of both up- and downstream model lengths
(6) grid dependency of results

Altogether 30 simulations were done to cover the two cases and the numerical variables. The transient flow simulations were continued until steady state and solution convergence were reached. For the scaled model simulations, 30–60 s were needed. The results were inspected for discharges and kinetic energy. The discharges at the inlet and outlet boundaries were monitored to calculate the mass imbalance, defined as difference between the two discharges normalized with the inlet discharge.

4 Results

The Flow3D simulation outputs were visualized graphically or saved as text files. The RNG turbulence model was compared with the experimental data, with a focus on discharges. Limited measurements of flow velocities and pressures were also used, which were taken at $y = 0.159$ m.

The numerical model successfully captured the pressurized flow (Case 1) and free surface flow (Case 2). Figures 3 and 4 compare the measured and simulated water surface profiles for both cases (G_s denotes mesh size and z_e elevation). The measurements did not cover the entire model length. There is a good agreement between the data set; however, the agreement is better for $x > 0.8$ m because of a higher reliability and accuracy in the measurements. The comparison is better defined using the relative error by taking the difference between simulation and experimental values and then dividing the results by the experimental values. An error range between 0.25% and 3.5% was found for both cases. Table 2 compares the measured and simulated discharges for Cases 1 and 2 and also lists the relative mass

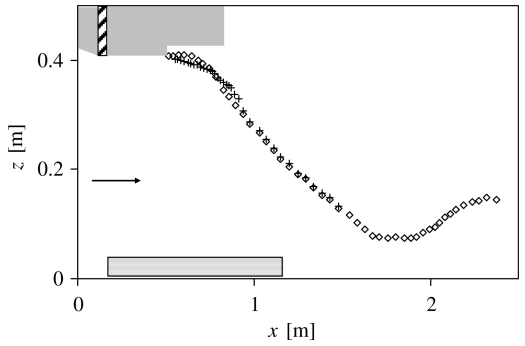

Figure 3 Comparison between simulated (◇ $L = 0.073$ m, $G_s = 0.016$ m) and (+) measured water surface profiles, Case 1 for $H_e = 1.045$ m

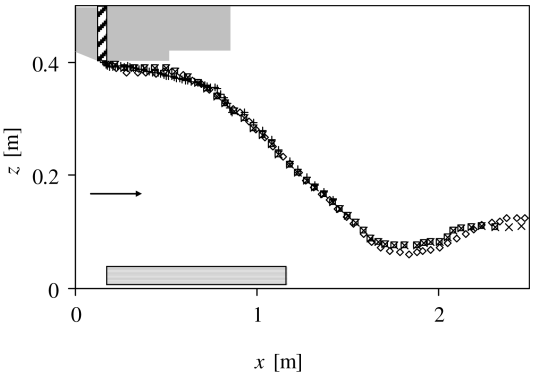

Figure 4 Comparison between simulated (◇ $L = 0.073$ m, $G_s = 0.01$ m; □ $L = 0.073$ m, $G_s = 0.016$ m; × $L = 0.0338$ m, $G_s = 0.016$ m) and (+) measured water surface profiles, Case 2 for $H_e = 1.045$ m

imbalances, resulting in good agreement with the experiments. The discharges are predicted within 1.4–4.6%. The relative mass imbalances were in the range of 0.5–1.5%. Figure 5 compares the simulated and measured discharges at $H_e = 113$ m for different gate openings. The discharges are normalized (Q_n) with discharge of the fully opened gate. The gate opening heights φ_n are normalized with a (Fig. 1). The agreement with the experimental data is good, with a maximum error of $\pm$ 1.5%. Inclusion of air entrainment in the simulations did not affect the discharges.

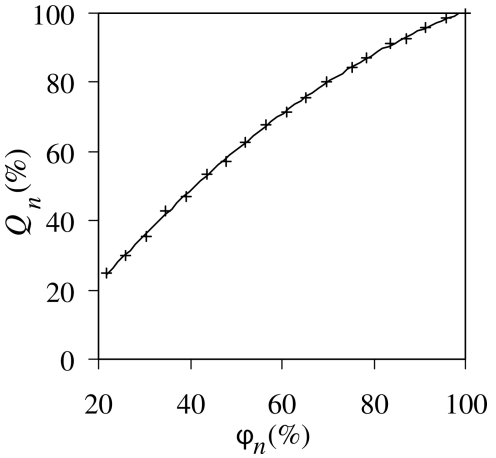

Figure 5 Comparison between (—) simulated and (+) measured normalized discharges at normalized gate openings, Case 1, $H_e = 113$ m ($H_{e,\text{model}} = 1.045$ m)

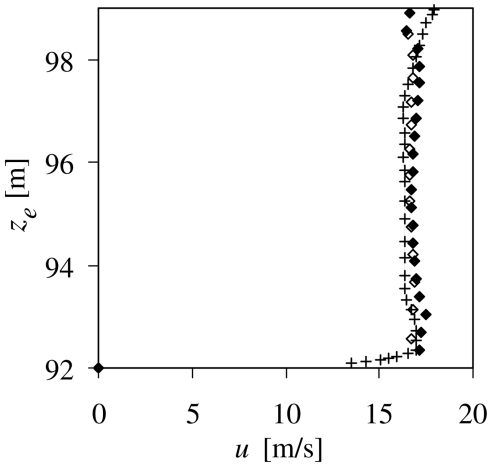

Figure 6 Comparison between simulated (◇ simulated scale model, ◆ simulated prototype) and measured velocity profile (+), section I, Case 2 for $H_e = 113$ m ($H_{e,\text{model}} = 1.045$ m)

Velocity and static pressure distributions showed good agreement. Figure 6 compares the streamwise velocity u profiles for Case 2 at section I (Fig. 1). The experimental data were upscaled to prototype scale. They are overestimated by 2.6%.

Table 2 Comparison between measured and simulated discharges for scale model 1:22

				Flow3D		
Case	H_e prototype scale (m)	Surface roughness (mm)	Discharge experiments ($m^3 s^{-1}$)	Mean discharge ($m^3 s^{-1}$)	Mass imbalance (%)	Relative error (%)
1	105	0.72	0.069	0.067	0.64	2.60
	107		0.078	0.075	0.58	4.00
	110		0.091	0.087	1.00	4.00
	113		0.103	0.098	1.50	4.10
2	105		0.063	0.066	0.28	4.60
	107		0.073	0.073	0	1.40
	110		0.085	0.088	−0.14	4.10
	113		0.094	0.098	0	4.60

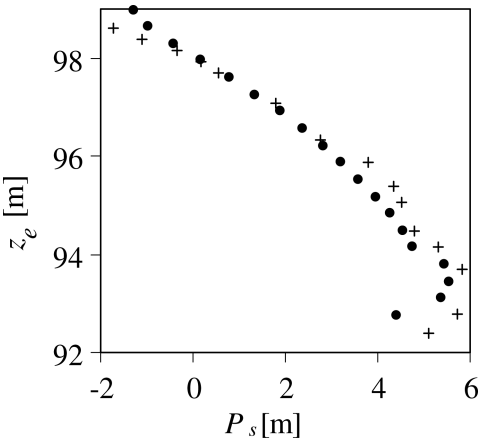

Figure 7 Comparison between (•) simulated and (+) measured pressure profiles at section I, Case 2 for $H_e = 113$ m ($H_{e,\text{model}} = 1.045$ m)

The agreement is better in the boundary layer near the wall. The static pressure P_s profile for Case 2 is compared with those of the experiments in Fig. 7. The agreement is good except at elevations below 93 m. However, for Case 1 (not shown), the pressures were overestimated by 10%. The inclusion of air entrainment in the simulations did not improve the agreement.

5 Discussion

The discharges are lower for free surface than for pressurized flow. Free surface flow separates from the upper edge of the bottom outlet (Fig. 4), because of the negative static pressure distribution (Fig. 7). In turn, the flow separation gives rise to an additional contraction coefficient C_c, which is the ratio of a to the flow depth at section II (Fig. 1), based on

$$Q = ab\mu_d C_c \sqrt{2g(H_e - C_c a)} \tag{1}$$

in which b represents width of bottom outlet; g, acceleration of gravity; and μ_d, discharge coefficient. For $H_e = 113$ m, $C_c \cong 0.916$. The corresponding value for pressurized flow is $C_c = 1$, such that the discharge is reduced by a factor of 0.925, comparable to the ratio of the two discharges, i.e. 0.918 (214/233, Table 1).

Hydraulic structure models are often based on the Froude similitude. Reynolds number-related scale effects are introduced, as the prototype Reynolds number is normally much larger than that of the model. The increase in the Reynolds number can affect the velocity distribution and the boundary layer properties. To examine this issue, the numerical scale models were up-scaled to prototype sizes and the simulations for the entire water levels were repeated for both Cases 1 and 2. Table 3 shows the simulation results in terms of discharge. Comparing Table 2 with Table 3, both the relative error and the mass imbalance are reduced for the prototype cases. There is a general increase in discharges of about 1%. However, the data do not provide any definite evidence of scale effects. One possible issue is the effect of surface roughness. Table 3 considers a smooth surface identical to the scale model. To address this issue, eight new simulations were done for equivalent roughness heights in the range from 5 to 15 mm, covering finished concrete surfaces (0.3–3 mm) and rough concrete surfaces (3–10 mm). The results were found independent from the surface roughness for rough concrete surfaces. However, the discharges were reduced for the high surface roughness of 15 mm, due to higher friction losses.

For partial gate closure, the discharge varies with the square of gate opening, whereas for a fully opened gate, discharge varies with $H_e^{1/2}$. The choices of turbulent length scale, the advection method, and the turbulence model are three important issues in CFD simulations of hydraulic structures. Using a high turbulent length scale increases the dynamic viscosity, which leads to over-prediction of diffusion, thereby causing large changes in the free-surface profile. The common approach is to use a value equal to 7% of a typical flow length scale. In the present study, the length scale was varied between 0.073 and 0.388 m, corresponding to 7% of

Table 3 Comparison between measured and simulated discharges at prototype scale

Case	H_e prototype scale (m)	Surface roughness (mm)	Discharge Experiments ($m^3\ s^{-1}$)	Mean flow discharge Flow3D ($m^3\ s^{-1}$)	Mass imbalance (%)	Relative error (%)
1	105	0.72	155	157	0.31	1.30
	107		178	179	0	0.90
	110		207	207	0.05	0.40
	113		233	231	1.12	0.90
	113[a]		233	230	−0.38	1.30
2	105		142	145	−0.64	2.40
	107		165	166	0.44	0.60
	110		192	195	0	2.40
	113		214	217	−0.36	1.40
	113*		214	216	−0.18	1.00

[a]Extended downstream length (from 55 to 80 m)

the flow depth or the hydraulic radius based on H_e and a (Fig. 1). The simulated water surface profiles were then found independent of the turbulent length scale (Fig. 4). One possible explanation for this insensitivity is related to the flow type. In accelerating flows, Reynolds shear stresses and turbulent kinetic energy levels decrease along the boundary layer when compared with the flat boundary layer. Bottom outlet flow is an accelerating flow type with damping turbulence effects thereby limiting the effect of length scale.

The choice of advection method was investigated for Case 1 and $H_e = 0.682$ m for both scale model and prototype. Using the first-order scheme, the relative error in predicting the discharge coefficient was found to be 2.5%. The error was reduced to 2% for the second-order scheme, but the CPU time significantly increased. The accuracy of the first-order scheme was therefore considered sufficient. Comparing the two turbulence models, the RNG model gave the results that are closest to those of the experimental data.

Increasing the upstream model extent did not improve the accuracy in predicting the discharges. This might be due to the choice of the hydraulic static pressure condition at the upstream model section. Velocity-based boundary conditions appear to be more sensitive to this extent. The flow condition at the downstream section was supercritical, thus increasing the downstream model length did not affect the results (Table 3). The possible reasons for discrepancies between the experimental and simulated results are experimental errors, errors in flow modelling, and errors in geometrical modelling:

1) *Experimental errors* The discharge measurements were more reliable because a simple, well-established method free from various instabilities and flow problems was used. The error range from 1.4% to 4.6% is comparable to 4.6% in discharge measurement. The simulated water surface profiles disagreed more from the experiments, especially in the confined region of the model. Water surface fluctuations caused by the flow separation at the edges were difficult to measure at the flume glass wall. Beyond the confined region, the water surface profiles had a smoother shape and thus were easier to measure. The errors in predicting the velocity and static pressure measurements are comparable to the experimental errors. One possible reason was uncertainties involved concerning the exact location of the measurement points. Pressure measurement could have been affected by the presence of air bubbles in the measuring device.
2) *Errors in flow modelling* are related to the numerical methods (discretization and iteration errors), boundary conditions, and the closure models. The mass imbalance reported can be related to this category. The Finite Volume Method is always conservative. However, the numerical errors associated with the discretization scheme for the convective term result in a difference between the in- and outflow (mass imbalance). The estimated total error is about 2%, including 0.5% error in using the first-order discretization scheme.
3) *Errors in geometrical modelling* involve the quality of model geometry. The transfer of the model drawings to a physical model may be more inaccurate than transferring the drawings to a CAD model. A mismatch in geometrical design between a CAD and a physical model can affect the boundary layer properties as well as the discharges. The latter modify the pressure and velocity distributions. The errors in this category are comparable to the first category.

6 Conclusions

Computational fluid dynamics is an effective tool in analysing free-surface flows of bottom outlets. Pressurized and free-surface flow features were accurately captured using the Volume Of Fluid method implemented in Flow3D. The transient flow features associated with a moving gate were successfully captured as well as the discharge characteristic for partial opening of the gate. The water surface profiles and the discharges were predicted within a relative small error range. The first-order momentum advection scheme gives sufficient accuracy for engineering purposes. The velocity and pressure distributions were predicted within a maximum error of 2.6% and 10%, respectively. The model performed with similar accuracy for both model and prototype cases.

Acknowledgements

The research was sponsored by the Swedish Hydropower Centre (SVC). The licence to use Flow3D was issued by Flow Science Inc., Santa Fe, NM, USA. The investigator has also benefited from useful suggestions made by the Flow3D support group, especially by Melissa Carter.

Notation

a = bottom outlet opening
b = width of bottom outlet
C_c = contraction coefficient
g = acceleration of gravity
G_s = mesh size
H_e = upstream flow depth
L = turbulent length scale
P_s = static pressure head
Q = flow discharge
Q_n = discharge normalized with discharge of fully opened gate
u = streamwise velocity
x, y, z = streamwise, spanwise, and vertical directions
z_e = elevation
μ_d = discharge coefficient
φ_n = gate opening height normalized with a

References

Bhajantri, M.R., Eldho, T.I., Deolalikar, P.B. (2007). Modeling hydrodynamic flow over spillway using weakly-compressible flow equations. *J. Hydraulic Res*. 45(6), 844–852.

Casey, M., Wintergerste, T. (2000). *Best practice guidelines*. European Research Community on Flow, Turbulence And Combustion, ERCOFTAC.

Cederwall, K., Bergh, H. (1982). ASWAN II: On hydraulic model studies 4: Discharge capacity of sluice. *Report* 18. Hydraulic Laboratory, Royal Institute of Technology, Stockholm.

Dargahi, B. (2004). Three-dimensional flow modelling and sediment transport in the River Klarälven. *Earth Surface Processes and Landforms* 29(7), 821–852.

Dargahi, B. (2006). Experimental study and 3D numerical simulations for a free-overflow spillway. *J. Hydraulic Engng*. 132(9), 899–907.

Flow3D (2006). User manual: Excellence in flow modeling, software version 9.1. FlowScience, Inc., Santa Fe N.M, USA.

Griffith, R.A., Rutherford, J.H., Alavi, A., Moore, D., Groeneveld, J. (2007). Stability review of the Wanapum spillway using CFD analysis. *Canadian Dam Association*, Bulletin, Fall 2007, 16–26.

Hirt, C.W., Nichols, B.D. (1981). Volume of fluid (VOF) methods for the dynamics of free boundaries. *J. Comp. Physics* 39, 201–225.

Hirt, C.W., Sicilian, J.M. (1985). A porosity technique for the definition of obstructs in rectangular cell meshes. Proc. 4th Intl. Conf. *Ship hydrodynamics*, 1 – 19. National Academy of Science, Washington DC.

Hirt, C.W. (1992). Volume-fraction technique: Powerful tools for flow modelling. *Report* FSI-92-00-02. Flow Science, Santa Fe NM.

Ho, D.K.H., Boyes, K.M., Donohoo, S.M. (2001). Investigation of spillway behaviour under increased maximum flood by computational fluid dynamics technique. 14th *Australasian Fluid Mechanics Conf*., Adelaide University, Adelaide, Australia, 10–14.

Ho, D.K.H., Cooper, B.W., Riddette, K.M., Donohoo, S.M. (2006). Application of numerical modeling to spillways in Australia. *Dam and reservoirs:* Societies and environment in the 21st century, 951-959. Taylor & Francis, London.

Kirkgoz, M.S., Akoz, M.S., Oner, A.A. (2009). Numerical modeling of flow over a chute spillway. *J. Hydraulic Res*. 47(6), 790–797.

Olsen, N.R.B., Kjellesvig, H.M. (1998). Three-dimensional numerical flow modelling for estimation of spillway capacity. *J. Hydraulic Res*. 36(5), 775–785.

Savage, B.M., Johnson, M.C. (2001a). Flow over ogee spillway: Physical and numerical model case study. *J. Hydraulic Engng*. 127(8), 640–649.

Savage, B.M., Johnson, M.C. (2001b). Physical and numerical comparison of flow over ogee spillway in the presence of tailwater. *J. Hydraulic Engng*. 132(12), 1353–1357.

Townson, J.M. (1991). *Free-surface hydraulics*. Unwin Hyman, London.

Unami, K., Kawachi-Babar, M.M., Itagak, H. (1999). Two-dimensional numerical model of spillway flow. *J. Hydraulic Engng*. 125(4), 369–375.